Earth Surf. Dynam. Discuss., 3, 285–326, 2015
www.earth-surf-dynam-discuss.net/3/285/2015/
doi:10.5194/esurfd-3-285-2015

Earth Surface Dynamics Discussions
Open Access

The periglacial engine of mountain erosion – Part 1: Rates of frost cracking and frost creep

J. L. Andersen[1], D. L. Egholm[1], M. F. Knudsen[1], J. D. Jansen[2], and S. B. Nielsen[1]

[1]Department of Geoscience, Aarhus University, Høegh-Guldbergs Gade 2, 8000 Aarhus C, Denmark
[2]Institute of Earth and Environmental Science, University of Potsdam, Germany

Received: 30 March 2015 – Accepted: 1 April 2015 – Published: 22 April 2015

Correspondence to: J. L. Andersen (jane.lund@geo.au.dk)

Published by Copernicus Publications on behalf of the European Geosciences Union.

Abstract

With accelerating climate cooling in the late Cenozoic, glacial and periglacial erosion became more widespread on the surface of the Earth. The resultant shift in erosion patterns significantly changed the large-scale morphology of many mountain ranges worldwide. Whereas the glacial fingerprint is easily distinguished by its characteristic fjords and U-shaped valleys, the periglacial fingerprint is more subtle but potentially prevailing in some landscape settings. Previous models have advocated a frost-driven control on debris production on steep headwalls and glacial valley sides. Here we investigate the important role that periglacial processes also play in less steep parts of mountain landscapes. Understanding the influences of frost-driven processes in low-relief areas requires a focus on the consequences of an accreting soil-mantle, which characterizes such surfaces. In this paper, we present a new model that quantifies two key physical processes: frost cracking and frost creep, as a function of both temperature and sediment thickness. Our results yield new insights to how climate and sediment transport properties combine to scale the intensity of periglacial processes. The thickness of the soil-mantle strongly modulates the relation between climate and the intensity of mechanical weathering and sediment flux. Our results also point to an offset between the conditions that promote frost cracking and those that promote frost creep, indicating that a stable climate can only provide optimal conditions for one of those processes at a time. Finally, quantifying these relations also opens the possibility of including periglacial processes in large-scale, long-term landscape evolution models, as demonstrated in a companion paper.

1 Introduction

Most of the Earth's mountain ranges show clear signs of glacial erosion, with distinct glacial landforms such as broad U-shaped valleys, hanging valleys and cirque-basins. Many of these mountain ranges have likely been thoroughly re-shaped during the late

ESURFD
3, 285–326, 2015

Cenozoic period, where the cooling climate allowed glaciers to form or expand, and erode into new parts of the landscape. Global cooling has also expanded the realm of other cold-climate processes, but their long-term influence on the shape of mountain ranges is less recognized and less well understood compared with the glacial fingerprint.

The steep headwall and sides of glacial valleys are examples of weathering-limited landforms where bedrock erosion may be controlled by frost activity. Previous studies have modelled the relations between temperature and frost-cracking processes in order to investigate the climatic control on frost-related debris production on steep slopes and on the distribution of threshold slopes (Hales and Roering, 2007, 2009; Scherler, 2014). These studies show a good correlation between the modelled zone of maximum frost-cracking intensity and the source area of scree production in the Southern Alps (Hales and Roering, 2007, 2009), and in the Khumbu Himalaya the base of the steepest headwalls correlates with zones of peak frost-cracking intensity, indicating frost-driven undercutting of these slopes (Scherler, 2014). Such findings together indicate that frost processes could be an important agent of erosion on steep mountain slopes.

It has been suggested that periglacial processes are also involved in the formation of the high and relatively smooth summit flats that characterize the alpine landscapes of, for example, the Laramide ranges in the western USA and the mountains of Scandinavia, Greenland, and eastern Canada (Small and Anderson, 1998; Marquette et al., 2004; Munroe, 2006; Nielsen et al., 2009) (Fig. 1). These low-relief surfaces, which are typically covered by a thin mantle of regolith, are the focus of mass wasting and diffusive processes during ice-free periods. Furthermore, ice masses are commonly observed to be cold-based in such high elevation settings and therefore tend to preserve rather than erode the underlying terrain (Briner and Swanson, 1998; Fabel et al., 2002; Stroeven et al., 2006; Goodfellow, 2007).

Using existing models to determine the periglacial influence on the summit flats is, however, not entirely straightforward because the low-angle slopes allow sediment to accumulate. Depending on their thickness, sediments are expected to influence frost

ESURFD
3, 285–326, 2015

cracking of underlying bedrock in two ways: (1) the sediments may prevent frost cracking because they dampen the propagation of surface temperature variations into the bedrock, and (2) they promote frost cracking by functioning as a high-porosity water-reservoir for the ice-segregation process that drives frost cracking. In order to quantify the efficiency of periglacial processes on these low-relief landforms, it is therefore vital to take a closer look at the sediment cover shielding bedrock from direct contact with the atmosphere (Anderson et al., 2012). In this study, we quantify for the first time the mechanical bedrock weathering through frost cracking for a range of sediment thicknesses as well as mean annual air temperatures. This gives us new insights into how sediment and temperature combine to scale frost-cracking intensity.

It has long been recognized that in soil-mantled landscapes, the denudation rate is governed by the rate at which soil can be transported downslope rather than by the weathering rate of the underlying bedrock (Gilbert, 1877). When modelling periglacial processes in soil-mantled landscapes, it is therefore essential to quantify the efficiency of the active processes of sediment transport. We therefore include an analysis of the efficiency of frost heave as a transport mechanism across a range of mean annual air temperature and sediment thickness. The quantification of both frost weathering and frost-driven transport also opens the possibility of incorporating these relations into a large-scale landscape evolution model. This enables us to explore the long-term feedbacks among climate, frost-weathering intensity, sediment mobility, and the evolution of mountain topography, as shown in an accompanying paper (Egholm et al., 2015).

2 Background

The term “periglacial” encompasses a range of processes that involve freezing and thawing in the cold, but non-glaciated realm of polar and alpine environments (French, 2013). There is still much to be learned about how these mechanisms work and at what scales (See Hall and Thorn, 2011, for a review), but here we focus on two par-

ESURFD
3, 285–326, 2015

ticular processes: frost cracking and frost creep, which are both relatively well-studied via physical experiments. Frost cracking was originally attributed to volume expansion (∼ 9 %) during freezing of water trapped in cracks and pores in the bedrock. However, more recent research has found that this mechanism requires very high levels of saturation and confinement and instead the experimental focus has shifted to another process, known as ice segregation (Hallet et al., 1991; Murton et al., 2006). The ice segregation process has long been known from studies on frost heave and creep of soils (e.g. Taber, 1929), but has also been proposed as a mechanism for breakdown of rock (Walder and Hallet, 1985, 1986). Ice segregation causes ice lenses to grow by freezing of water that is drawn from the surrounding rock or sediment during periods of sustained subfreezing temperatures. The water migrates to the ice lenses through films of water at the grain-pore-interface (Rempel et al., 2004).

Information on frost cracking and frost creep comes primarily from cold-room laboratory experiments where small amounts of sediment or rock are subjected to multiple cycles of freezing and thawing (e.g. Taber, 1929; Matsuoka, 1990; Hallet et al., 1991; Murton et al., 2006). Furthermore, field monitoring has established empirical relationships between the frost-cracking process and natural temperature variations (e.g. Matsuoka, 2008; Amitrano et al., 2012; Girard et al., 2013). Several theoretical models have simulated freezing of water in porous media (Walder and Hallet, 1985; Vlahou and Worster, 2010), but only a few studies have attempted to model the spatial extent of periglacial processes in relation to climate. Anderson (1998) developed the first model relating frost cracking to climatic parameters. He introduced the concept of the frost-cracking window (FCW) (−8 to −3 °C) based on results by Walder and Hallet (1985) and quantified frost-cracking intensity (FCI) as the length of time spent in this window during an annual temperature cycle. Hales and Roering (2007, 2009) extended this model by quantifying frost cracking in bedrock as a function of the temperature gradient when temperature falls within the FCW. This model, furthermore, requires that water is available in the direction of warming, which allows for continuous transport of

ESURFD
3, 285–326, 2015

water to the zone of frost cracking (since ice segregation can only cause water to flow from warm to cold areas).

Hales and Roering (2007) quantified FCI as a function of mean annual air temperature by depth-integrating frost cracking during an annual cycle. Anderson et al. (2012) extended this model by including diurnal temperature oscillations, the effect of latent heat on temperatures, a transient snow cover, a regolith layer with adjustable porosity and a constant thickness (0.4 m), as well as limitations to water transport through frozen bedrock. The work presented here builds on these previous models and extends them by systematically delineating the effect of the thickness of the sediment cover on frost-cracking and frost-creep processes.

3 Approach

We present a mechanistic model that quantifies the influence of temperature and sediment cover on the two key periglacial processes: (1) production of mobile regolith from bedrock via frost cracking, and (2) transport of sediment by frost creep. In order to provide a sensitivity analysis, we compute the intensity of frost cracking (FCI) and the frost-heave induced transport diffusivity (κ) for combinations of the mean annual air temperature (MAT) and thickness of sediment overlying the bedrock (S). Our approach to computing FCI and κ is based on Anderson et al. (2012), with some important modifications.

3.1 The heat equation

Because frost cracking and frost creep take place within a limited temperature range, quantification of these processes requires knowledge of how changes in atmospheric temperature are propagated into the ground. We therefore solve the one-dimensional

ESURFD
3, 285–326, 2015

transient heat equation for conduction of heat within the upper 20 m of the subsurface:

$$C\frac{\partial T}{\partial t} = \frac{\partial}{\partial z}\left(k\frac{\partial T}{\partial z}\right) + H_{\mathrm{L}}, \quad (1)$$

where T is the temperature; C is the bulk volumetric heat capacity; k is bulk conductivity, and t is time. H_{L} is the latent heat release or consumption by phase change of water. We assume that the only heat exchanged in the system is caused by conductive heat flow, and we therefore ignore the thermal effect of fluid advection. The heat equation is solved by the finite-element method, which allows for irregular discretization and for accurately incorporating discontinuous variations in thermal properties, such as that between water-saturated sediment and bedrock. We use the possibility of irregular discretization to increase the model resolution close to the surface where the temperature gradient can be large (Fig. 2).

A constant heat flux from the Earth's interior, q_{b}, is used as a boundary condition at the bottom of the profile ($z = 20$ m). At the surface, the temperature is forced to vary annually as a sinusoidal oscillation around a given MAT with a superimposed diurnal sinusoidal variation (Fig. 3); the amplitude of the annual variation is $\mathrm{d}T_{\mathrm{a}}$, while the diurnal variation has a random amplitude between 0 and $\mathrm{d}T_{\mathrm{d}}$ (Table 1). The MAT is translated directly into ground surface temperature.

The presence of water and ice influences the thermal properties of rock and sediment, and the parameters ρ, c, and k hence depend on porosity, ϕ, and water fraction, w_{f}. Based on porosity and the properties of bedrock, ice, and water, we first use standard mixing rules (Ling and Zhang, 2004; Anderson et al., 2012) to compute the conductivity and heat capacity for the frozen (k_{f} and C_{f}) and the unfrozen situation (k_{u}

ESURFD
3, 285–326, 2015

and C_u):

$$k_u = k_w^{\phi} k_r^{1-\phi}, \quad (2)$$

$$k_f = k_i^{\phi} k_r^{1-\phi}, \quad (3)$$

$$C_u = \phi C_w + (1-\phi) C_r, \quad (4)$$

$$C_f = \phi C_i + (1-\phi) C_r, \quad (5)$$

where k_w, k_i and k_r are the conductivities of water, ice and bedrock, respectively. C_w, C_i, and C_r are the volumetric heat capacities for the same three materials. We then mix these parameters according to water fraction (w_f) in order to obtain the bulk parameters:

$$k = k_u^{w_f} k_f^{1-w_f}, \quad (6)$$

$$C = w_f C_u + (1-w_f) C_f. \quad (7)$$

The effects of latent heat, H_L, can be simulated by increasing the specific heat capacity if the pore-water is in the process of changing phase (Ling and Zhang, 2004). Equation (1) is then replaced by the simplification:

$$\widetilde{C} \frac{\partial T}{\partial t} = \frac{\partial}{\partial z} \left(k \frac{\partial T}{\partial z} \right), \quad (8)$$

with

$$\widetilde{C} = \begin{cases} C + \frac{\phi \rho_w}{dT_L} L & \text{for } 0 < w_f < 1 \\ c & \text{else} , \end{cases} \quad (9)$$

where L is the specific latent heat of water and dT_L is the width of the temperature window in which phase changes occur. We follow this strategy, and increase the specific

ESURFD
3, 285–326, 2015

heat capacity in elements where freezing or thawing occur based on the criteria:

$$\text{Freezing:} \quad T < 0\,^{\circ}\text{C and } w_{\text{f}} > 0, \tag{10}$$

$$\text{Thawing:} \quad T > -1\,^{\circ}\text{C and } w_{\text{f}} < 1. \tag{11}$$

Note that the two criteria are overlapping if $-1\,^{\circ}\text{C} < T < 0\,^{\circ}\text{C}$ and $0 < w_{\text{f}} < 1$. In this case, both freezing and thawing may occur depending on the sign of H_{L}. We compute H_{L} by combining Eqs. (1) and (8):

$$H_{\text{L}} = (C - \widetilde{C})\frac{\partial T}{\partial t} \tag{12}$$

and relate this to water fraction by considering the heat involved in freezing and thawing:

$$\frac{\partial w_{\text{f}}}{\partial t} = -\frac{H_{\text{L}}}{\phi \rho_{\text{w}} L} = \frac{1}{\mathrm{d}T_{\text{L}}}\frac{\partial T}{\partial t}. \tag{13}$$

The water fraction of each element can now be updated by integration of Eq. (13).

The effect of latent heat is clear from the evolution of the thermal profiles, mainly because latent heat exchange stalls the propagation of temperature changes around zero degrees. The effect is strongest when the porosity is high, for example in the case where bedrock is covered by a thick layer of porous sediment (Fig. 3).

3.2 Quantifying frost-cracking intensity

Our model for frost cracking is based on ice-segregation theory (see Murton et al., 2006; Vlahou and Worster, 2010, for reviews). Ice-segregation growth has been shown to operate primarily in the temperature interval from −8 to −3 °C (Walder and Hallet, 1986; Anderson, 1998). Furthermore, in order for ice lenses to grow, water must be available and able to flow towards the ice lenses. This requires a continuous positive thermal gradient (increasing temperature) from the ice lenses to the water. Because

ESURFD
3, 285–326, 2015

the magnitude of the thermal gradient determines the flow rate of the water, Hales and Roering (2007) suggested that frost-cracking intensity scales with the thermal gradient in situations where water is available along a path following the positive thermal gradient. Anderson et al. (2012) supplemented this approach with a penalty function that reduces frost cracking efficiency dependent upon the distance that water must migrate through low-permeable frozen bedrock to reach the ice lenses. We continue along this line of thought by scaling the frost-cracking intensity with the magnitude of the thermal gradient multiplied by the volume of water available to the ice-segregation growth process:

$$\mathrm{FCI}(z,t) = \begin{cases} \left|\frac{\mathrm{d}T}{\mathrm{d}z}\right| V_{\mathrm{w}}(z) & \text{if } -8\,^{\circ}\mathrm{C} < T < -3\,^{\circ}\mathrm{C} \\ 0 & \text{else} \end{cases} \tag{14}$$

Here $\mathrm{FCI}(z,t)$ is the cracking intensity at time t and depth z below the surface.

The water volume available for ice-segregation growth, V_{w}, is calculated by integrating the occurrence of water along the path, ℓ, that starts at depth z and follows the positive thermal gradient:

$$V_{\mathrm{w}}(z) = \int_{\ell} \phi(z') w_{\mathrm{f}}(z') e^{-\Gamma(z')} \mathrm{d}z'. \tag{15}$$

Note that ℓ is either up or down along the vertical profile, depending on the sign of the thermal gradient. ℓ extends from depth z to either (i) the surface, (ii) the profile bottom, or (iii) the point where the thermal gradient changes sign. Following Anderson et al. (2012), we apply a penalty function $e^{-\Gamma(z')}$ that depends on the distance the water must migrate to arrive at the point of ice segregation. This function depends on the properties of the material located between the water (at z') and the point of ice segregation (z). We therefore compute $\Gamma(z')$ by integrating the flow resistance, γ, from

ESURFD
3, 285–326, 2015

z to z':

$$\Gamma(z') = \int_{z}^{z'} \gamma(z'')\mathrm{d}z''. \quad (16)$$

We note that applying a constant value for γ ($2\,\mathrm{m}^{-1}$) results in a penalty function identical to that used by Anderson et al. (2012). However, because ice segregation occurs at temperatures below $-3\,^{\circ}\mathrm{C}$ and water is available only for higher temperatures, water must always flow through a mixture of frozen or unfrozen bedrock or sediment. We therefore use four different values for γ to characterize the permeability of (i) unfrozen sediment, (ii) frozen sediment, (iii) unfrozen bedrock, and (iv) frozen bedrock (Table 1). We also note that $e^{-\Gamma(z')} \to 0$ for $z' \to D$, which ensures that the existence of the profile bottom does not limit the water volume available for the cracking process.

By incorporating a measure for the actual amount of water present in the pore spaces of bedrock and sediment, we capture an important effect of the frost-cracking process: that sediment overlying bedrock acts as a water reservoir. The porosity of sediments is significantly higher than for bedrock, and V_{w} therefore increases rapidly if an unfrozen sediment layer exists in proximity to frozen bedrock. Yet, we suggest that the positive effect of water availability only increases up to a critical water volume, $V_{\mathrm{w}}(z) \leq V_{\mathrm{cw}}$ (Table 1), which defines the situation when the frost-cracking process is no longer limited by the availability of water. In Sect. 4.3, we explore the sensitivity of the model to the assumptions made regarding water availability.

Finally, the annually averaged frost-cracking intensity, $\overline{\mathrm{FCI}}$, is computed by depth-integrating the cracking intensity and averaging this depth-integrated value throughout a year:

$$\overline{\mathrm{FCI}} = \frac{1}{T_{\mathrm{a}}} \int_{0}^{T_{\mathrm{a}}} \int_{0}^{D} \mathrm{FCI}(z,t)\mathrm{d}z\mathrm{d}t, \quad (17)$$

ESURFD
3, 285–326, 2015

where T_a is one year and $D = 20$ m is the thickness of the profile.

3.3 Quantifying frost creep

Frost heave results from the expansion of (silt-sized) sediment when subjected to freezing and associated ice-lens growth. The expansion due to freezing is perpendicular to the slope of the surface while the thaw-conditioned contraction is vertical owing to gravity. The surface-parallel displacement of sediment arises from this angle discrepancy between directions of expansion and contraction (Fig. 4) (Anderson, 2002), a process noted long ago (Davison, 1889).

The contribution to horizontal sediment transport is:

$$\boldsymbol{Q} = -\beta z \mathrm{d}z \nabla h, \tag{18}$$

if a sediment layer of thickness dz located at depth z experiences a full freeze–thaw event. Here $\nabla h = [\frac{\partial h}{\partial x}, \frac{\partial h}{\partial y}]$ is the bed topographic gradient and β is the relative expansion of the layer when frozen (Fig. 4). The dimension of $\boldsymbol{Q}$ is m^2 as it records the volume of sediments advected in one full frost-heave event per unit width of the hillslope. We note that the dependency on z arises from the fact that expansion of a buried sediment layer causes passive transport of all sediments above this layer.

Formulating this in terms of the water fraction yields:

$$\boldsymbol{Q} = -\left[\frac{1}{2}\int_t \left|\frac{\partial w_\mathrm{f}}{\partial t}\right| \mathrm{d}t\right] \beta z \mathrm{d}z \nabla h, \tag{19}$$

where $\frac{1}{2}\int_t \left|\frac{\partial w_\mathrm{f}}{\partial t}\right| \mathrm{d}t = 1$ if the integral covers the full period of the frost-heave event, because a full frost-heave cycle involves shifting the water fraction from 1 to 0 and back to 1 again. However, unlike Eq. (18), Eq. (19) also captures the effect of partial frost-heave events, which may be important for the frost-creep rate if the MAT is close

ESURFD
3, 285–326, 2015

to the freezing point. When integrating the contributions from all sediment elements along the vertical profile and averaging the total frost-heave activity per year, we get the following annually-averaged sediment flux [$m^2\,a^{-1}$]:

$$\boldsymbol{q} = -\left[\frac{\beta}{2T_a}\int_0^{T_a}\int_0^{S}\left|\frac{\partial w_f}{\partial t}\right| z\,dz\,dt\right]\nabla h. \tag{20}$$

We can now formulate the sediment frost-creep process as a standard hillslope transport law:

$$\frac{\partial S}{\partial t} = -\nabla\cdot\boldsymbol{q}, \tag{21}$$

where

$$\boldsymbol{q} = -\kappa\nabla h \tag{22}$$

and

$$\kappa = -\frac{\beta}{2T_a}\int_0^{T_a}\int_0^{S}\left|\frac{\partial w_f}{\partial t}\right| z\,dz\,dt \tag{23}$$

is the transport efficiency [$m^2\,a^{-1}$], and S is the local sediment thickness.

4 Results

4.1 Rates of frost cracking

The modelled FCI shows that frost cracking can occur under very diverse climatic conditions depending on sediment thickness, and that the effect of sediment cover on frost-cracking rates depends on climate (Figs. 5 and 6).

ESURFD
3, 285–326, 2015

The model results point to peaks in frost-cracking activity in three distinct environments.

Firstly, frost cracking can occur in a relatively warm climate (MAT > 0 °C), where the temperature drops below zero only during the coldest nights in winter (Fig. 5b). The rapid diurnal temperature variations result in a shallow but very steep temperature gradient where temperatures in the frost-cracking window occur at the surface. At the same time, positive temperatures, and hence water, exist at only 20–30 cm depth below the surface (Fig. 7a). Since there is no water present at the surface, the water necessary for frost cracking comes from within the bedrock and the resulting frost-cracking intensity thus depends critically on the water migration capacity of the bedrock (parameters γ_{bc} and γ_{bw} in Table 1). As the freezing front does not penetrate far into the ground, the FCI is dampened by any sediment, which prevents the bedrock from reaching temperatures in the frost-cracking window. This effect is further enhanced by the larger water content of the sediment that stalls the freezing front because of latent heat. Frost cracking in this environment can therefore only occur where the sediment cover is very thin (≤ 20 cm) or absent (Fig. 5b and line 3 in Fig. 6a).

Secondly, frost cracking is promoted in an environment where the deep subsurface is frozen (MAT < 0 °C), but where surface temperatures rise above the melting point during summer and on warm days in spring/autumn (Figs. 5 and 7b). The water driving frost cracking in this setting comes from the surface, because the deeper ground is permanently frozen and because the annual temperature oscillation ensures a negative thermal gradient (temperatures decrease with depth) during summer periods, driving water downwards from the surface. Because the water comes from above, the presence of a sediment layer may accelerate cracking due to its water-holding capacity. On the other hand, the relatively large penetration depth (~ 2 m) of the annual temperature oscillation results in a rather gentle temperature gradient, and the distance between the positive temperatures at the surface and the bedrock within the FCW is a few meters (Fig. 7b). The most efficient frost cracking therefore takes place at the sediment–bedrock interface. Optimal conditions for frost cracking occur where the lower limit of

ESURFD
3, 285–326, 2015

the sediment coincides with the depth to the FCW, and this causes the FCI in cold environments to peak under a sediment cover 1–2 m thick.

Thirdly, frost cracking also occurs in very cold climates (MAT $\leq -8\,^{\circ}$C), where only the warmest days in summer experience surface temperatures above 0 °C. This is reflected in the tail of the FCI distribution towards relatively thin sediment covers for very cold temperatures (Fig. 5a). The low temperatures limit the amounts of water generated at the surface, and the transport of water is restricted through the frozen sediment and bedrock below. Frost cracking thus only occurs due to the large but shallow thermal gradient generated by the diurnal temperature variation (Fig. 7c). As a result, sediment thickness is critical; a thin sediment layer ($\leq$ 10–20 cm) promotes cracking owing to its water content, whereas thicker sediment ($\geq$ 20 cm) limits cracking because the transport path of water down to the top of the bedrock becomes too long. The colder the environment is, the shallower the sediment cover must be to accommodate frost cracking in the top of the bedrock.

Frost cracking in our model is very limited for MATs just below zero degrees, an outcome common to previous models (Hales and Roering, 2009; Anderson et al., 2012). This result may seem counter-intuitive, but at just below zero MAT the mean annual ground temperature is higher than the FCW. Temperatures required for frost cracking are therefore restricted to near-surface zones in winter; a time when the deeper subsurface is frozen and there is no water available. Conversely, when water does become available in summer, subsurface temperatures are too warm for frost cracking. Hence, frost-cracking activity is suppressed although temperatures oscillate around zero degrees. The temperature variation does, however, lead to efficient sediment transport by frost creep as demonstrated in the next section, and the model results thus point to an offset between the MATs that promote efficient frost cracking and those that promote transport by frost creep.

ESURFD
3, 285–326, 2015

4.2 Rates of frost creep

The modelled frost-transport efficiency (Fig. 8) shows the combined result of frequent, but shallow mass movement caused by the diurnal temperature variations and the larger but less frequent movement caused by deep penetration of the annual temperature oscillation. The contribution of the diurnal oscillations is minor, and the overall pattern is largely controlled by two properties related to the annual temperature oscillation.

Firstly, the maximum penetration depth of the freezing/thawing front depends on how close the MAT is to the phase change envelope (−1 to 0 °C). For thermal profiles with MATs close to the phase change envelope, the front penetrates to greater depths in the subsurface. Because sediment is passively transported on top of the thawing layer, a deep-seated phase-change event leads to greater mass movement than a shallower phase-change event. This effect is most clearly seen at sediment thicknesses above a few meters (Fig. 8). For a constant sediment thickness, the transport decreases with distance from the phase-change envelope (Fig. 8c).

Secondly, the maximum transport rate for any particular MAT (along lines parallel to the *S* axis in Fig. 8) occurs when the sediment thickness corresponds to the maximum penetration depth of the freezing/thawing front. At sediment thicknesses less than optimal thickness, freezing or thawing continues into the underlying bedrock, which does not increase the transport. The transport efficiency in this interval is limited by the sediment thickness and thus increases until the optimum sediment thickness is reached (Fig. 8b). For sediment thicknesses exceeding optimal thickness, the frost-transport efficiency is limited by the penetration depth of the freezing/thawing front and a plateau is attained with no further increase in transport efficiency. The optimal sediment thickness is highest for MATs close to the phase change envelope (−1–0 °C), where the annual temperature variation causes the deepest penetration of the freezing/thawing front.

The diurnal temperature oscillations extend the MAT interval for which transport occurs to more extreme temperature values. For these extreme temperatures, transport

ESURFD
3, 285–326, 2015

occurs in shallow sediment packages only because the surface temperatures on warm summer days or cold winter nights support freezing or thawing.

4.3 Model sensitivity

The modelled rates of frost cracking and frost creep reflect the basic assumptions and chosen parameters in the model. A different set of parameters may lead to different results. In this section, we therefore explore and discuss the sensitivity of the model results to variations in the most important parameters and assumptions.

4.3.1 Thermal properties

The frost-cracking intensity and the efficiency of frost-driven sediment transport are both highly dependent on the modelled temperature profiles. The parametrization of the thermal model therefore has a significant influence on the predicted rates of sediment transport and bedrock weathering.

While variations in thermal conductivity and specific heat capacity have only minor influence on the rates of frost cracking and frost creep, the amplitude of the annual temperature oscillation, dT_a, has a significant impact. dT_a is highly variable in natural environments and varies over time due to changes in climate. In general, dT_a increases with distance from the coast and from the equator (Legates and Willmott, 1990).

Increasing dT_a in the model leads to higher values of both FCI and sediment transport efficiency, κ (Fig. 9). It also leads to frost cracking and transport at a wider range of MATs, as well as to frost cracking for thicker sediment cover. For example, the FCI for MAT = −10 °C increases almost two orders of magnitude when dT_a is raised from 6 to 12 °C. It is therefore important to incorporate knowledge of dT_a when estimating frost-cracking rates in areas of unusually high or low annual temperature variations.

ESURFD
3, 285–326, 2015

4.3.2 Effect of a snow cover

We simulate the first-order effect of snow cover by reducing the amplitude of the diurnal temperature oscillations in winter (Fig. 10a). The motivation for this is that thick snow insulates the ground below and dampens the propagation of any high-frequency air temperature variations. Through this mechanism, the inclusion of snow cover has a significant effect on the rates of both frost cracking and sediment transport.

Because the frost-cracking intensity in positive MAT environments depends on cold temperatures at night in winter, the FCI is lowered substantially when diurnal variations are dampened. With a snow cover present, efficient frost cracking thus only occurs for cold temperatures (MAT $< -5\,^{\circ}\mathrm{C}$) under sediment covers up to 3 m thick (Fig. 10b).

The frost-creep efficiency (κ) is less affected, but for high, positive MATs ($> 5\,^{\circ}\mathrm{C}$) the sediment transport is reduced when the diurnal winter oscillations are dampened by snow cover. Diurnal temperature variations that cause short-lived freezing events during winter nights drive the sediment transport for high MATs. Even without a snow cover, the induced transport is modest because the frost propagates only a few centimetres into the ground, but with snow cover present the transport mechanism becomes negligible in this temperature interval.

4.3.3 Water availability

Water is essential for driving frost cracking at subzero temperatures, but the implementation of the water-dependency differs among existing models. In the following, we briefly review the different approaches and discuss the sensitivity of our results to how water-availability is quantified.

To account for the influence of water on frost-cracking rates, Hales and Roering (2007, 2009) included the condition that positive temperatures should be present somewhere in the temperature profile for frost cracking to take place. They also scaled the FCI with the temperature gradient, which is thought to determine the flow rate of water. Anderson et al. (2012, p. 306) argued that the growth rate of cracks should be lim-

ESURFD
3, 285–326, 2015

ited not only by the flow rate, but also by "the distance water must be moved through cold materials to get to the site of potential frost cracking". Based on this idea, they introduced a penalty function that makes the FCI decay exponentially with the distance between the zone of frost cracking and the positive temperatures. This implementation is in accordance with experimental results, indicating that "an external moisture source close to a freezing rock contributes to ice segregation" (Matsuoka, 2001, p. 304). In line with these results, we suggest that FCI should scale with not only migration distance, but also the amount of accessible water in the profile. Furthermore, we suggest that water should be limited more when it flows through cold bedrock, than when it flows through warm sediment. We have therefore integrated the available water and included varying flow restrictions based on the thermal state and porosity of the material. However, since these various ways of implementing water dependency are uncertain, we document the influence of our parametrization approach by exploring the FCI-patterns that arise from a range of other parameter choices (Fig. 11). Note that the scale of the FCI is orders of magnitude different for the various implementations, but in the following discussion we focus on differences in the general pattern.

In the first case, we follow Hales and Roering (2007) and allow frost cracking to take place only when water is present along a continuous thermal gradient (Fig. 11a); there is no dependency on migration distance or amount of water. This implementation gives rise to a very sharp boundary in frost-cracking intensity at 0 °C, as also seen in the original model by Hales and Roering (2007). Frost cracking just below 0 °C MAT is low because temperatures at the bottom of the profile reflect the MAT and when these are negative and do not contain much water, frost cracking goes down. However, as soon as MAT and thus the bottom-profile temperature rise above 0 °C, the frost-cracking intensity increases to very high values. This happens because the frost cracking in this case is not restricted by the long water migration distance, or the low amounts of water present. Furthermore the maxima in FCI under a few meters of sediment for frost cracking at negative MAT disappears, because the effect of a nearby water source stored in the sediment is removed.

ESURFD
3, 285–326, 2015

In the second case, the flow restriction of water is set to a constant level ($2\,m^{-1}$) independent of the porosity or thermal state of the elements (Fig. 11b). This leads to less dampening of the positive FCI with thickening sediment cover (compared to Fig. 5), because the flow in cold bedrock is less restricted. This illustrates that crack propagation in bedrock with a high fracture density can be very efficient leading to a positive feedback between the degree of rock damage and frost-cracking susceptibility.

In the third case (Fig. 11c), the FCI depends on the distance from an element in the FCW to the closest water (similar to Anderson et al., 2012), whereas the amount of water available within the profile has no effect. The flow restriction of water is again constant ($2\,m^{-1}$), independent of the porosity or thermal state of the elements. FCI at negative temperatures and with thick sediment is low because of the relatively long distance to available water and because there no longer is a contributing effect of a porous water-filled sediment layer.

Frost-cracking intensity in our model scales with the volume of water available (Eq. 14), but only up to a fixed limit, V_{cw} (Table 1). We chose this implementation because we believe that water availability can limit frost cracking only up to a certain threshold. Although the value for V_{cw} (4 cm) is not supported by empirical data, our experiments reveal that rates of frost cracking and sediment transport are rather insensitive to variations in V_{cw}. Only when V_{cw} is significantly reduced does it affect the computed FCI values, first as a reduction of FCI for positive MATs (V_{cw} = 5 mm) and then by also lowering frost cracking for negative MATs (V_{cw} = 1 mm).

4.3.4 Temperature thresholds for frost cracking

Finally we look at the influence of the chosen temperature thresholds for frost cracking defined by the frost-cracking window. Matsuoka (2001) summarises the experimental frost-cracking results for various rock types and reports frost cracking for high-porosity rocks (tuff, shale, chalk) from −5 to 0 °C and for medium-porosity rocks (limestone, sandstones) between −6 and −3 °C. Walder and Hallet (1985) predicted frost cracking

ESURFD
3, 285–326, 2015

via ice segregation in the interval between −4 and −15 °C for a marble and a granite. Together these observations and models indicate that the thresholds for frost cracking are more gradual and lithology-dependent than that suggested by the fixed implementation of the frost-cracking window from −8 to −3 °C suggests. We applied a range of FCW thresholds (some are shown in Fig. 12) and found that the lower boundary of the FCW does not affect the frost-cracking pattern appreciably, unless the total width of the window becomes very narrow (< 1 °C). It also shows (perhaps unsurprisingly) that raising the upper threshold for frost cracking lead to frost cracking at higher MAT.

5 Discussion

5.1 The rates of frost cracking

Including the effects of variable sediment thickness in numerical models of frost cracking generates new insights into how climate and sediment cover combine to control bedrock weathering rates. First, when studying the modelled values for FCI along the MAT-dimension (Fig. 6c), it is possible to compare our results to those of previous models. In the following, we thus compare the FCI results presented in this paper with the model introduced by Hales and Roering (2007, 2009) and that by Anderson et al. (2012).

While the Hales and Roering (2009) model includes two distinct zones of efficient frost cracking, one for negative MATs and one for positive MATs, Anderson et al. (2012) suggested that only the cold-region cracking could survive penalties to water transport in cold bedrock. Our model generally confirms the findings of Anderson et al. (2012), although we suggest that frost cracking can still be active in moderately warm climates, provided that the sediment cover is sufficiently thin (< 10 cm) and the surface temperature is occasionally lowered into the FCW (Fig. 6c). Frost cracking under warm conditions is, however, very sensitive to bedrock water saturation, because water driving the frost cracking at positive temperatures must come from within the bedrock during

ESURFD
3, 285–326, 2015

freezing of the surface in winter. The warm region cracking is also potentially limited by snow cover that insulates the bedrock from the cold atmosphere in winter (Fig. 10). Given that hillslope angle governs the likelihood of retaining snow cover as well as a sediment layer, our model indicates that in warm-regions active frost cracking will be restricted to winter and primarily on steep and wet bedrock surfaces, such as along valley sides and valley headwalls.

5.2 Soil production function

It is generally accepted that the conversion of bedrock to sediment is related to the thickness of the sediment mantle, and that if enough sediment accumulates, generation of new sediment will stall or cease (Heimsath et al., 1997). However, the exact nature of this relation (soil production function) has been debated (see Humphreys and Wilkinson, 2007, for a review). Some have argued for an exponential decline in sediment production rate with thickening sediment cover (Dietrich et al., 1995; Heimsath et al., 1997), while others favour a relation in which soil production rate peaks (the "humped" function) under a finite sediment thickness (Gilbert, 1877; Carson and Kirkby, 1972; Wilkinson et al., 2005). The strongest argument for the latter model is that a thin sediment layer is more likely to retain moisture, which is a vital ingredient for physical and chemical weathering, whereas bare bedrock promotes run-off and remains dry much of the time.

In warmer climates, empirical support for both the exponential function and humped functions have been proposed. Empirical results from soil-mantled slopes have supported the exponential decay model (Heimsath et al., 1997). Anderson (2002), however, argued for a humped soil-production model, to explain the presence of tors (bedrock knobs) observed at hill crests. According to Anderson (2002), the tors protrude due to the divergence of sediment from the crest, which leaves the summits bare. The erosion at hill crests must therefore be slower compared to the surrounding soil-mantled slopes in order to explain the presence of these tors.

ESURFD
3, 285–326, 2015

Assuming that sediment production scales with frost-cracking intensity, our results suggest that the shape of the soil-production function strongly depends on temperature (Fig. 6). For positive MATs, sediment production decays exponentially with thickening sediment cover (line 3 in Fig. 6a). We note that this result rely on the assumption that moisture is present at all times. A variable moisture content in the outer decimetres of bare bedrock as suggested by Sass (2005), could potentially influence the frost-cracking intensity for bare bedrock, an effect that is not captured by the present model. For negative MATs, sediment production first increases with sediment thickness (up to 1–2 m) and then decays exponentially with further sediment mantle thickening (lines 1 and 2 in Fig. 6a). The optimal sediment thickness (for which sediment production is maximised) decreases with decreasing MAT. Our model thus suggests that both end-member soil-production functions may be viable in the periglacial environment, with long-term temperature fluctuations likely to result in complicated soil chronosequences.

5.3 Frost creep and depth-dependent transport

High-frequency diurnal temperature variations represent the main driver of frost creep for thin sediment covers. The diurnal temperature variations do not penetrate far into the sediment and the freeze–thaw events that they cause are shallow and frequent. For sediment covers less than 1 m thick, the most efficient transport (highest κ) hence occur for MATs around −6 and +6 °C (Fig. 8a and c), because diurnal variations generate the highest number of freeze–thaw events for these thermal settings (Anderson et al., 2012). However, the annual temperature variation becomes more dominant for thicker mantles (> 1 m), and its influence on creep is maximized for MATs around 0 °C (Fig. 8a and b). This is because the seasonal temperature variation is slow enough to penetrate much deeper into the sediment. Freeze–thaw in a deep sediment layer contributes far more to the sediment flux than shallow events because the overlying sediment pile is passively transported when the deep layer expands and contracts.

The efficiency of sediment transport by frost creep (κ) principally depends on sediment thickness, because the frequency of freeze–thaw events decreases with depth

ESURFD
3, 285–326, 2015

into the sediment (Fig. 8). Although sediment flux initially increases with sediment thickness for all MATs, it saturates at a temperature-dependent limiting thickness, beyond which it becomes constant akin to linear hillslope diffusion models (Fig. 8b). This type of sediment-thickness-dependent function is in close agreement with the hypothesized transport-function by Anderson (2002), but is driven by MAT. For MATs around 0 °C, the annual temperature variation causes freezing and thawing up to 3 m into the sediment, whereas the freeze–thaw penetration-depth is more limited under warmer and colder conditions, respectively. We therefore emphasize that our frost-creep model supports a transport-function rooted in sediment thickness (e.g. Braun et al., 2001; Heimsath et al., 2005; Johnstone and Hilley, 2015) up to a limit of ~ 3 m for MAT ~ 0 °C and < 1 m for colder and warmer settings.

5.4 Limits to water availability?

Is it necessary to penalize frost-cracking intensity by water availability? Scaling frost-cracking intensity with the temperature gradient of the section within the FCW already (partly) accounts for dragging water to the FCW, because the water content in a porous media is not zero at sub-freezing temperatures. Water will be drawn to the zone of potential frost cracking provided that a hydraulic connection exists between the ice forming in the FCW and moisture elsewhere in the profile via a film of unfrozen water along grain boundaries (pre-melted films). The thickness of the pre-melted films gradually decreases with colder temperatures and because the temperature gradient drives the suction force, it also determines the flow rate of water. Nonetheless, experimental results suggest that a nearby water source increases frost-cracking intensity (Matsuoka, 2001), thereby justifying the implementation of additional penalties to water transport distance.

ESURFD
3, 285–326, 2015

6 Conclusions

We present a 1-D thermal model that quantifies sediment production via frost cracking of bedrock, and sediment transport via frost creep as functions of mean annual temperature and sediment cover thickness. The key findings are as follows:

1. The relation between MAT and frost cracking is strongly modulated by the thickness of a sediment layer. For negative MATs (in the range −4 to −10 °C) frost-cracking intensity can be enhanced by the presence of a sediment layer, whereas for moderately positive MATs (0–9 °C) the presence of a sediment layer can significantly dampen the frost-cracking intensity.

2. Whereas frost-cracking intensity peaks at MATs slightly above and below the freezing point, frost transport is most intense at MATs corresponding to the phase-change of water. This offset may have important implications for the evolution of hillslopes in periglacial landscapes (an effect explored by Egholm et al., 2015).

3. Our model for frost cracking and frost creep is driven by temperature variations in the subsurface, whereas the presence of moisture – another prerequisite for frost-driven processes – is neglected. Any systematic deviations in moisture content should therefore be taken into account before transferring the model to natural systems.

The Supplement related to this article is available online at doi:10.5194/-15-285-2015-supplement.

Author contributions. J. L. Andersen and D. L. Egholm designed the study, developed the model code, performed the simulations, and produced the figures. J. L. Andersen prepared the manuscript with contributions from all co-authors.

ESURFD
3, 285–326, 2015

Acknowledgements. This work was supported by the Danish Council for Independent Research. J. D. Jansen was supported by a Discovery Grant from the Australian Research Council (DP130104023).

References

Amitrano, D., Gruber, S., and Girard, L.: Evidence of frost-cracking inferred from acoustic emissions in a high-alpine rock-wall, Earth Planet. Sc. Lett., 341, 86–93, 2012. 289

Anderson, R. S.: Near-surface thermal profiles in alpine bedrock: implications for the frost weathering of rock, Arctic Alpine Res., 30, 362–372, 1998. 289, 293

Anderson, R. S.: Modeling the tor-dotted crests, bedrock edges, and parabolic profiles of high alpine surfaces of the Wind River Range, Wyoming, Geomorphology, 46, 35–58, 2002. 296, 306, 308

Anderson, R. S., Anderson, S. P., and Tucker, G. E.: Rock damage and regolith transport by frost: an example of climate modulation of the geomorphology of the critical zone, Earth Surf. Proc. Land., 38, 299–316, doi:10.1002/esp.3330, 2012. 288, 290, 291, 294, 295, 299, 302, 304, 305, 307, 325

Braun, J., Heimsath, A. M., and Chappell, J.: Sediment transport mechanisms on soil-mantled hillslopes, Geology, 29, 683–686, 2001. 308

Briner, J. P. and Swanson, T. W.: Using inherited cosmogenic ^{36}Cl to constrain glacial erosion rates of the Cordilleran ice sheet, Geology, 26, 3–6, 1998. 287

Carson, M. A. and Kirkby, M. J.: Hillslope Form and Process, vol. 475, Cambridge University Press, Cambridge, 1972. 306

Davison, C.: On the creeping of the soilcap through the action of frost, Geol. Mag., 6, 255–261, 1889. 296

Dietrich, W. E., Reiss, R., Hsu, M.-L., and Montgomery, D. R.: A process-based model for colluvial soil depth and shallow landsliding using digital elevation data, Hydrol. Process., 9, 383–400, 1995. 306

Egholm, D. L., Andersen, J. L., Knudsen, M. F., Jansen, J. D., and Nielsen, S. B.: The periglacial engine of mountain erosion – Part 2: Modelling large-scale landscape evolution, Earth Surf. Dynam. Discuss., 3, 327–369, doi:10.5194/esurfd-3-327-2015, 2015. 288, 309

ESURFD

3, 285–326, 2015

Fabel, D., Stroeven, A. P., Harbor, J., Kleman, J., Elmore, D., and Fink, D.: Landscape preservation under Fennoscandian ice sheets determined from in situ produced ^{10}Be and ^{26}Al, Earth Planet. Sc. Lett., 201, 397–406, 2002. 287

French, H. M.: The Periglacial Environment, John Wiley & Sons, West Sussex, England, UK, 2013. 288

Gilbert, G.: Report on the geology of the Henry Mountains, US Geographical and Geological Survey, Washington Government Printing Office, USA, Rocky Mountain Region, 1877. 288, 306

Girard, L., Gruber, S., Weber, S., and Beutel, J.: Environmental controls of frost cracking revealed through in situ acoustic emission measurements in steep bedrock, Geophys. Res. Lett., 40, 1748–1753, doi:10.1002/grl.50384, 2013. 289

Goodfellow, B.: Relict non-glacial surfaces in formerly glaciated landscapes, Earth-Sci. Rev., 80, 47–73, 2007. 287

Hales, T. and Roering, J. J.: Climatic controls on frost cracking and implications for the evolution of bedrock landscapes, J. Geophys. Res., 112, F02033, doi:10.1029/2006JF000616, 2007. 287, 289, 290, 294, 302, 303, 305, 325

Hales, T. and Roering, J. J.: A frost "buzzsaw" mechanism for erosion of the eastern Southern Alps, New Zealand, Geomorphology, 107, 241–253, 2009. 287, 289, 299, 302, 305

Hall, K. and Thorn, C.: The historical legacy of spatial scales in freeze–thaw weathering: misrepresentation and resulting misdirection, Geomorphology, 130, 83–90, 2011. 288

Hallet, B., Walder, J., and Stubbs, C.: Weathering by segregation ice growth in microcracks at sustained subzero temperatures: verification from an experimental study using acoustic emissions, Permafrost Periglac., 2, 283–300, 1991. 289

Heimsath, A. M., Dietrich, W. E., Nishiizumi, K., and Finkel, R. C.: The soil production function and landscape equilibrium, Nature, 388, 358–361, 1997. 306

Heimsath, A. M., Furbish, D. J., and Dietrich, W. E.: The illusion of diffusion: field evidence for depth-dependent sediment transport, Geology, 33, 949–952, 2005. 308

Humphreys, G. S. and Wilkinson, M. T.: The soil production function: a brief history and its rediscovery, Geoderma, 139, 73–78, 2007. 306

Johnstone, S. A. and Hilley, G. E.: Lithologic control on the form of soil-mantled hillslopes, Geology, 43, 83–86, 2015. 308

Legates, D. R. and Willmott, C. J.: Mean seasonal and spatial variability in global surface air temperature, Theor. Appl. Climatol., 41, 11–21, 1990. 301

ESURFD
3, 285–326, 2015

Ling, F. and Zhang, T.: A numerical model for surface energy balance and thermal regime of the active layer and permafrost containing unfrozen water, Cold Reg. Sci. Technol., 38, 1–15, 2004. 291, 292
Marquette, G. C., Gray, J. T., Gosse, J. C., Courchesne, F., Stockli, L., Macpherson, G., and Finkel, R.: Felsenmeer persistence under non-erosive ice in the Torngat and Kaumajet mountains, Quebec and Labrador, as determined by soil weathering and cosmogenic nuclide exposure dating, Can. J. Earth Sci., 41, 19–38, 2004. 287
Matsuoka, N.: The rate of bedrock weathering by frost action: field measurements and a predictive model, Earth Surf. Proc. Land., 15, 73–90, 1990. 289
Matsuoka, N.: Microgelivation versus macrogelivation: towards bridging the gap between laboratory and field frost weathering, Permafrost Periglac., 12, 299–313, 2001. 303, 304, 308
Matsuoka, N.: Frost weathering and rockwall erosion in the southeastern Swiss Alps: long-term (1994–2006) observations, Geomorphology, 99, 353–368, 2008. 289
Munroe, J. S.: Investigating the spatial distribution of summit flats in the Uinta Mountains of northeastern Utah, USA, Geomorphology, 75, 437–449, 2006. 287
Murton, J. B., Peterson, R., and Ozouf, J.-C.: Bedrock fracture by ice segregation in cold regions, Science, 314, 1127–1129, 2006. 289, 293
Nielsen, S. B., Gallagher, K., Leighton, C., Balling, N., Svenningsen, L., Jacobsen, B. H., Thomsen, E., Nielsen, O. B., Heilmann-Clausen, C., Egholm, D. L., Summerfield, M. A., Clausen, O. R., Piotrowski, J. A., Thorsen, M. R., Huuse, M., Abrahamsen, N., King, C., and Lykke-Andersen, H.: The evolution of western Scandinavian topography: a review of Neogene uplift versus the ICE (isostasy–climate–erosion) hypothesis, J. Geodyn., 47, 72–95, 2009. 287
Rempel, A. W., Wettlaufer, J., and Worster, M.: Premelting dynamics in a continuum model of frost heave, J. Fluid Mech., 498, 227–244, 2004. 289
Sass, O.: Rock moisture measurements: techniques, results, and implications for weathering, Earth Surf. Proc. Land., 30, 359–374, 2005. 307
Scherler, D.: Climatic limits to headwall retreat in the Khumbu Himalaya, eastern Nepal, Geology, 42, 1019–1022, 2014. 287
Small, E. E. and Anderson, R. S.: Pleistocene relief production in Laramide mountain ranges, western United States, Geology, 26, 123–126, 1998. 287
Stroeven, A., Harbor, J., Fabel, D., Kleman, J., Hättestrand, C., Elmore, D., Fink, D., and Fredin, O.: Slow, patchy landscape evolution in northern Sweden despite repeated ice-sheet flaciation, Geol. S. Am. S., 398, 387–396, doi:10.1130/2006.2398(24), 2006. 287

ESURFD
3, 285–326, 2015

Taber, S.: Frost heaving, J. Geol., 37, 428–461, 1929. 289
Vlahou, I. and Worster, M. G.: Ice growth in a spherical cavity of a porous medium, J. Glaciol., 56, 271–277, 2010. 289, 293
Walder, J. and Hallet, B.: A theoretical model of the fracture of rock during freezing, Geol. Soc. Am. Bull., 96, 336–346, 1985. 289, 304
Walder, J. S. and Hallet, B.: The physical basis of frost weathering: toward a more fundamental and unified perspective, Arctic Alpine Res., 18, 27–32, 1986. 289, 293
Wilkinson, M. T., Chappell, J., Humphreys, G. S., Fifield, K., Smith, B., and Hesse, P.: Soil production in heath and forest, Blue Mountains, Australia: influence of lithology and palaeoclimate, Earth Surf. Proc. Land., 30, 923–934, 2005. 306

ESURFD
3, 285–326, 2015

Table 1. Model parameters. Unless otherwise specified, these values apply to all model results.

Symbol	Description	Value
dT_a	Amplitude of annual surface temperature variation	8 °C
dT_d	Max. amplitude of diurnal temperature variation	4 °C
γ_{sw}	Flow restriction in warm sediment	$1.0\,m^{-1}$
γ_{sc}	Flow restriction in cold sediment	$2.0\,m^{-1}$
γ_{bw}	Flow restriction in warm bedrock	$2.0\,m^{-1}$
γ_{bc}	Flow restriction in cold bedrock	$4.0\,m^{-1}$
V_{cw}	Critical water volume	$0.04\,m^2$
ϕ_s	Porosity sediment	0.30
ϕ_{br}	Porosity bedrock	0.02
q_b	Basal heat flow	$0.05\,W\,m^{-2}$
k_w	Conductivity water	$0.56\,W\,m^{-1}\,K^{-1}$
k_i	Conductivity ice	$2.14\,W\,m^{-1}\,K^{-1}$
k_r	Conductivity bedrock	$3.0\,W\,m^{-1}\,K^{-1}$
c_w	Volumetric heat capacity water	$4210\,kJ\,kg^{-1}\,K^{-1}$
c_i	Volumetric heat capacity ice	$1880\,kJ\,kg^{-1}\,K^{-1}$
c_r	Volumetric heat capacity bedrock	$2100\,kJ\,kg^{-1}\,K^{-1}$
β	Frost-heave expansion coefficient	0.05
L	Specific latent heat of water	$333.6\,kJ\,kg^{-1}$

ESURFD
3, 285–326, 2015

Figure 1. Low-relief summit area at Ranastongi, Southern Norway, 1900 m a.s.l. Wide-spread sorting patterns in the blocky debris surrounding the summit suggest periglacial processes are either active re-distributors of sediment on this surface today or have been so in the recent past. But do periglacial processes also have long-term effects on the topographic development of low-relief surfaces like this? Photo: Christian Brædstrup.

ESURFD
3, 285–326, 2015

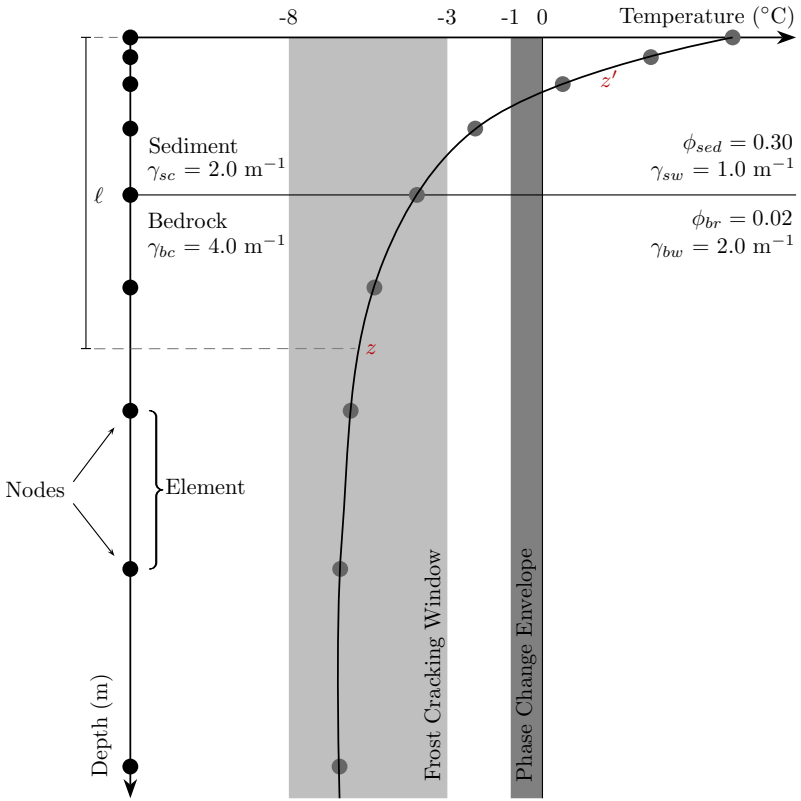

Figure 2. Schematic of the model setup. The water volume available for frost cracking in an element at depth z in the frost-cracking window is found by multiplying the porosity, ϕ, the water fraction, w_f, and the integrated flow resistance, Γ, of all elements along the path ℓ. The integrated flow resistance from an element containing water (z') to z, is found by integrating the element flow resistance (γ) multiplied by the thickness of each element along the path between z and z'. The magnitude of γ depends on the thermal state and porosity of each element; bc = cold bedrock, bw = warm bedrock, sc = cold sediment, sw = warm sediment.

ESURFD
3, 285–326, 2015

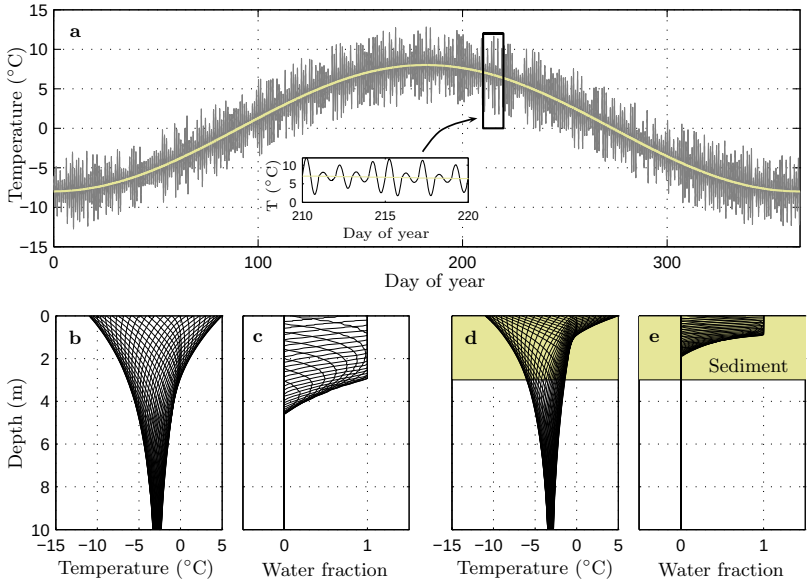

Figure 3. (a) The temperature curve used as the surface boundary condition for the heat equation. The curve is a sinusoidal annual temperature oscillation of amplitude $dT_a = 8\,^{\circ}C$. Superimposed on this curve are diurnal sinusoidal variations of random amplitude between 0 and 4 °C. The inset shows details of the two superimposed variations. **(b)** Modelled temperature profiles shown at weekly intervals throughout a year. The diurnal oscillations are in this case omitted for clarity. Latent heat exchange stalls the propagation of temperature variations, and this leads to a kink in the temperature profiles around 0 °C. **(c)** The corresponding weekly evolution of water fraction along the profile. A water fraction of 0 corresponds to frozen conditions and 1 to completely thawed sediment/bedrock. The partially thawed part of the profile (water content between 0 and 1) extends deeper than the 0 °C isotherm, because ice starts to thaw at −1 °C. (**d** and **e**) As for (**b** and **c**) but with a sediment cover (yellow fill). Note that the effects of the latent heat are more pronounced because the sediment has more porosity than bedrock. The latent heat dampens the propagation of temperature variations into the subsurface and the freeze–thaw events are shallow in the case of thick sediment cover.

ESURFD
3, 285–326, 2015

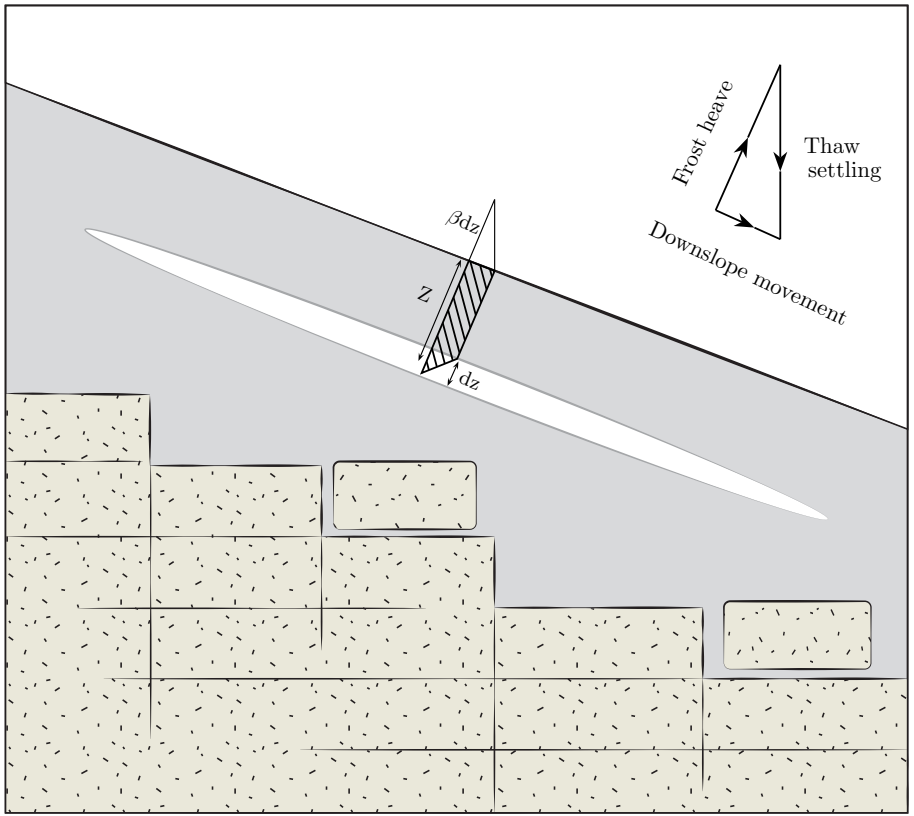

Figure 4. Sketch of the frost-creep mechanism. The down-slope movement of sediment (grey) occurs due to the angle-discrepancy between frost heave and thaw settling. The white area marks a zone of thickness dz that expands and contracts (by βdz). The down-slope sediment flux caused by this freeze–thaw event is represented by the hatched area. Note that the expansion has been exaggerated for illustration purposes, in the model β is 0.05.

ESURFD
3, 285–326, 2015

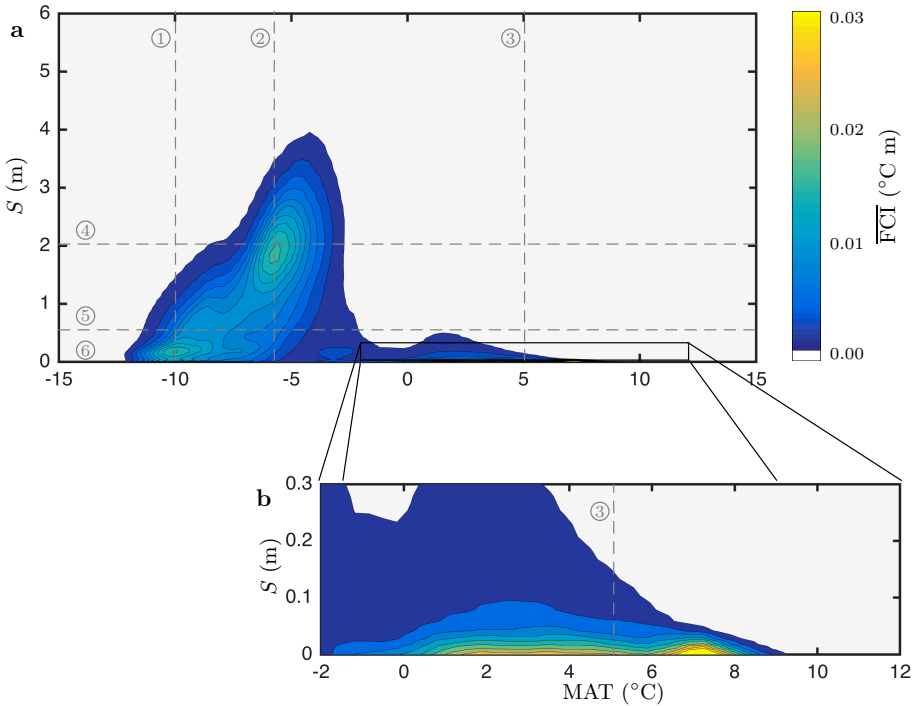

Figure 5. The integrated frost-cracking intensity, $\overline{\text{FCI}}$, as a function of mean annual temperature, MAT, and sediment thickness, S. Each point in the contour plot corresponds to the annually integrated $\overline{\text{FCI}}$ for a particular combination of MAT and S. The contour plot was constructed from 8100 such combinations. The porosity of both sediment and bedrock is assumed to be 100 % saturated by water. The dashed lines with numbers correspond to transects that are shown in Fig. 6. The inset shows the $\overline{\text{FCI}}$ for positive MATs in detail. Here $\overline{\text{FCI}}$ is strongly limited by sediment thickness and decays rapidly when S increases to more than a few cm.

ESURFD
3, 285–326, 2015

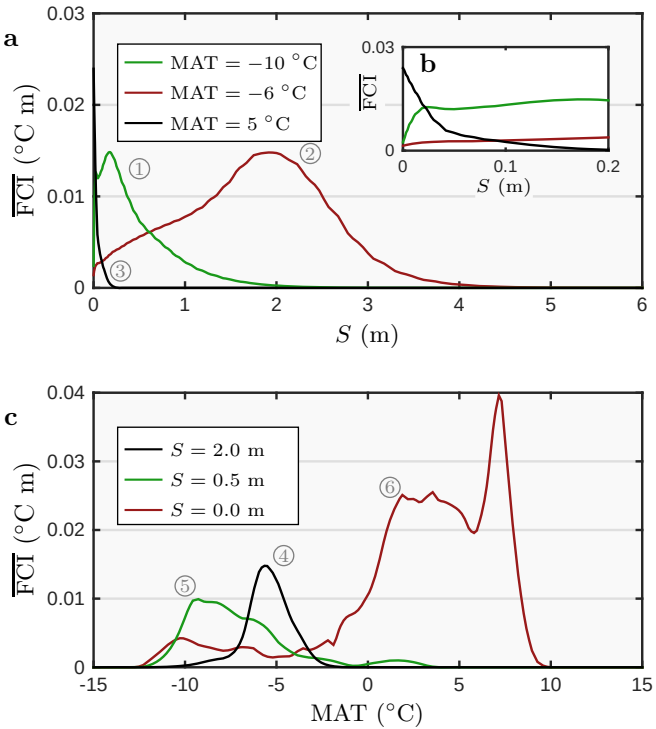

Figure 6. The integrated frost-cracking intensity along profiles shown in Fig. 5. **(a)** Profiles along the S axis illustrate how $\overline{\text{FCI}}$ depends on sediment thickness for three different MATs. Note the exponential decay function for MAT = 5 °C and the "humped" function for the two colder settings. **(b)** Inset highlighting the change in $\overline{\text{FCI}}$ for thin sediment cover. **(c)** Profiles of $\overline{\text{FCI}}$ parallel to the MAT axis showing how the effects of climate depend on sediment thickness. Areas with no or very little sediment cover (red line) have the highest $\overline{\text{FCI}}$ in warm regions, where rapid freezing events in winter promote intense cracking. In regions with permafrost (MAT < 0 °C), frost cracking is most intense under thicker sediments.

ESURFD
3, 285–326, 2015

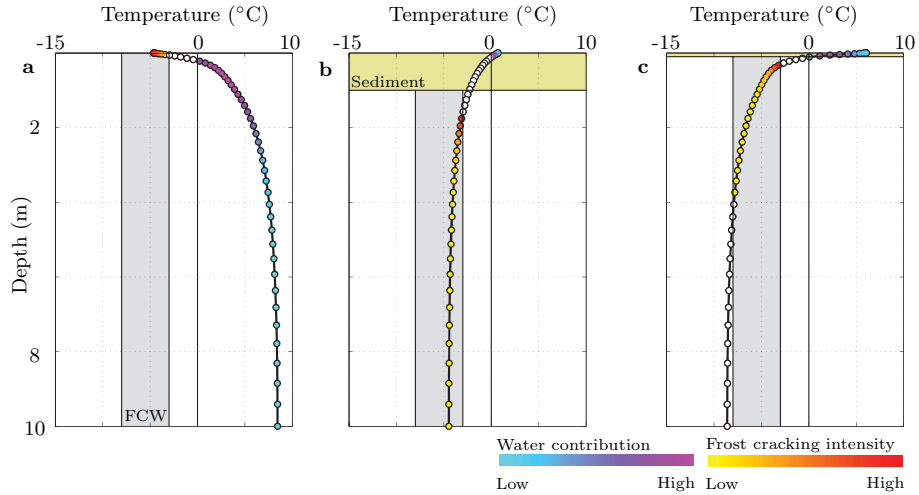

Figure 7. Three examples of temperature profiles under different field scenarios. The circles mark the position of finite-element nodes: blue-violet colors indicate zones that contribute water; red-yellow colors indicate zones with active frost cracking. The grey temperature interval marks the frost-cracking window (FCW). **(a)** A warm, bare bedrock setting with MAT = 8 °C and therefore no permafrost. Frost cracking occurs very close to the surface when the temperatures drop into the FCW in winter. **(b)** A colder situation with permafrost and MAT within the FCW (MAT = −4.5 °C). Frost cracking takes place a few meters below the surface at the bottom of the active layer. By providing water the sediment cover (yellow fill) promotes frost cracking until the sediment thickness exceeds the active-layer thickness. **(c)** A situation with extensive permafrost and MAT below the FCW (MAT = −8.5 °C). Frost cracking is now most active close to the surface in summer. Again, because water must come from above the FCW, a thin sediment layer amplifies frost cracking. The white circles are nodes that are outside the FCW and that do not contribute water.

ESURFD
3, 285–326, 2015

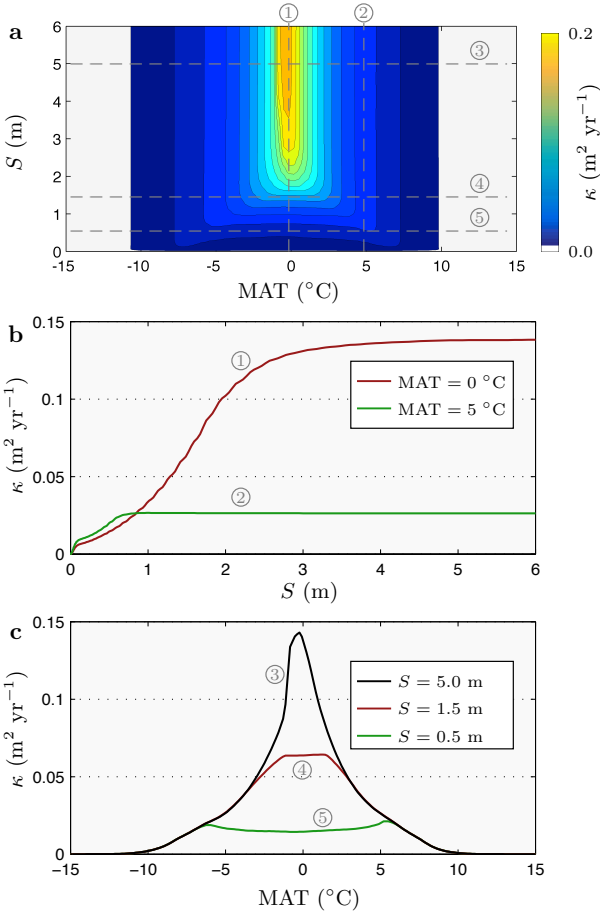

Figure 8. (a) Contours of the integrated frost-creep efficiency, κ, as a function of MAT and sediment thickness, S. Locations of transects plotted in (**b** and **c**), are shown with grey, dashed lines and numbers.

ESURFD
3, 285–326, 2015

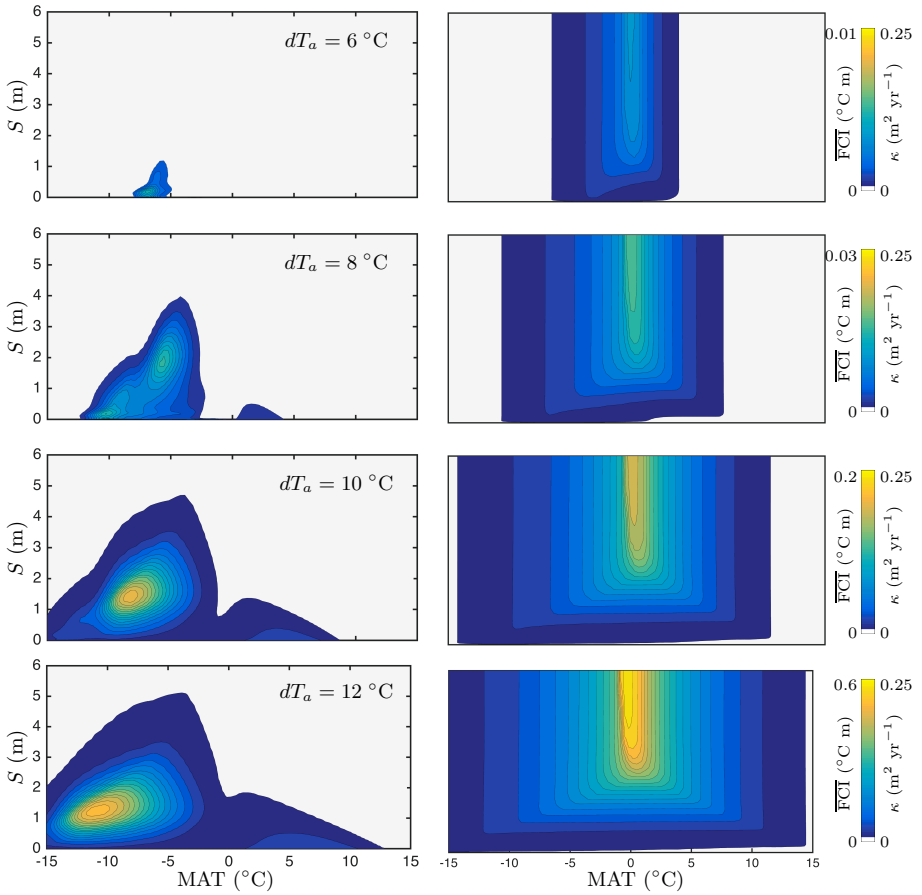

Figure 9. The effect of the amplitude of the annual temperature variation, dT_a, on frost cracking (left) and frost creep (right). Note that the color-scale for $\overline{\text{FCI}}$ varies between situations with different dT_a.

ESURFD
3, 285–326, 2015

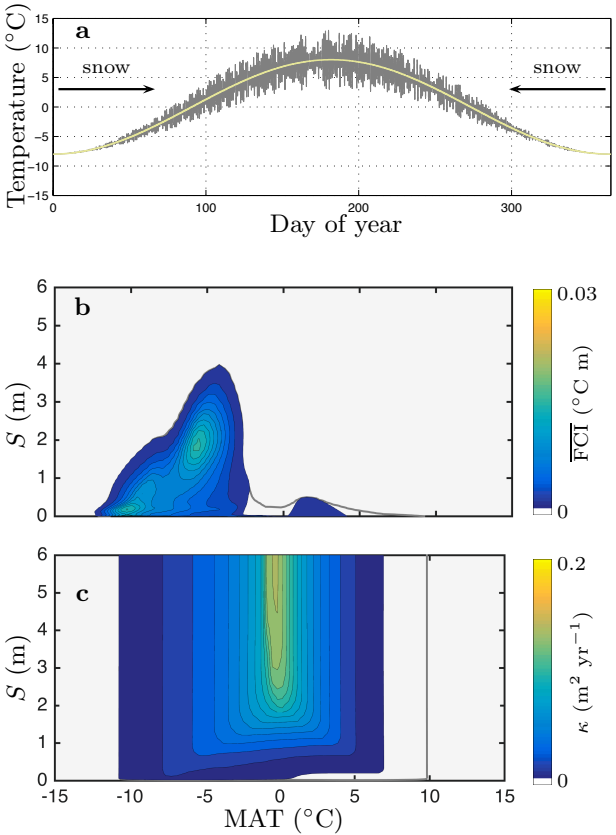

Figure 10. (a) A simulated snow cover dampens the amplitude of the diurnal temperature variations at the surface in winter. **(b)** The snow cover effect limits the integrated frost cracking for MATs around and above 0 °C. The lowest contour level of Fig. 5 is indicated with a black line for easy comparison. **(c)** The snow cover reduces the frost-creep efficiency at positive MATs, because the sediment is insulated from the cold air temperatures on cold nights in winter. Again, the black line represents the lowest contour level of Fig. 8.

ESURFD
3, 285–326, 2015

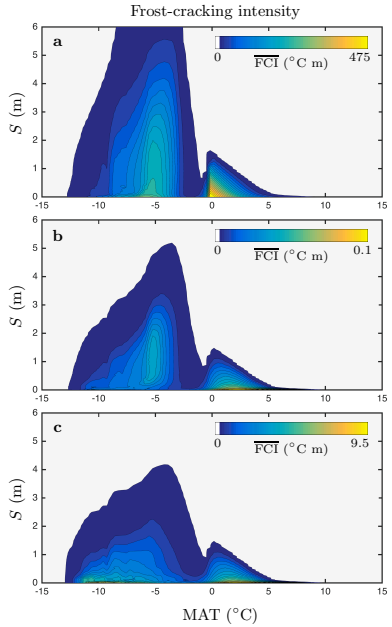

Figure 11. The integrated frost-cracking intensity as a function of sediment thickness and MAT, for varying water-penalty implementations. **(a)** Frost cracking occurs wherever water is present along the vertical profile in the direction of warming temperature. Compared to our standard model (Fig. 5), the FCI does not depend on the distance to, or amount of water available at the source. This model implementation is similar to the model by Hales and Roering (2007). **(b)** The distance to the water source and the amount of water available influences the penalty function, but in contrast to our standard model, the flow-restriction parameters, γ, are constant ($2\,m^{-1}$) and independent of the porosity or thermal state. **(c)** Flow restriction parameters are constant ($2\,m^{-1}$), and the distance between an element in the FCW and the nearest water source scales the FCI. Compared to our standard model, the FCI is unaffected by the amount of water available at the source (the porosity is not accounted for). This model implementation is similar to that of Anderson et al. (2012).

ESURFD
3, 285–326, 2015

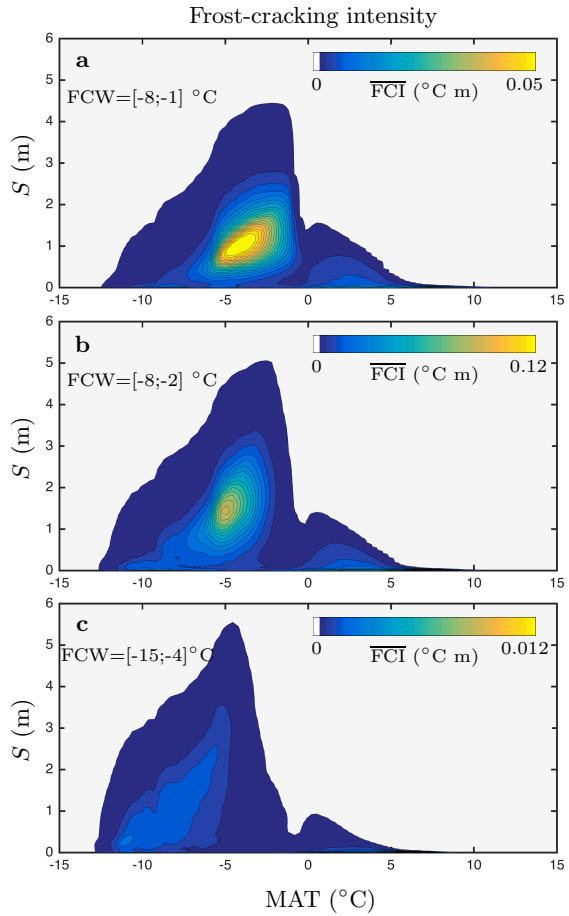

Figure 12. Integrated frost-cracking intensity as a function of sediment thickness and MAT, for frost-cracking windows of **(a)** [−8;−1]˚C **(b)** [−8;−2]˚C and **(c)** [−15;−4]˚C. Note the different color scales.

ESURFD
3, 285–326, 2015